



# Resonance Spectra of Coplanar Waveguide MKIDs Obtained Using Frequency Sweeping Scheme

M. Nagai<sup>1</sup> · Y. Murayama<sup>1,2</sup> · T. Nitta<sup>2,3</sup> · H. Kiuchi<sup>1</sup> · Y. Sekimoto<sup>4</sup> · H. Matsuo<sup>1</sup> · W. Shan<sup>1</sup> · M. Naruse<sup>5</sup> · T. Noguchi<sup>6</sup>

Received: 16 August 2019 / Accepted: 8 November 2019 / Published online: 19 November 2019  
© Springer Science+Business Media, LLC, part of Springer Nature 2019

## Abstract

We are developing a detector array for astronomical observations in the 100-GHz band using microwave kinetic inductance detectors (MKIDs) and a readout system for the array with frequency sweeping scheme, which uses a frequency sweeping probe signal instead of a fixed-frequency probe signal. This scheme enables us to simultaneously obtain the resonance spectra of MKIDs in an array and to derive the resonance frequencies corresponding to the power of incoming radiation. It has the advantage of the dynamic range being higher than the standard scheme and the derived resonance frequencies not being affected by changes of the gain or delay in the transmission line. The resonance profile measured, however, can be distorted by frequency sweeping, and hence, it is necessary to evaluate the effect of frequency sweeping on the resonance spectrum. We made measurements using the scheme with several frequency-sweep velocities and checked its effect on the resonance frequency and the quality factor. A slow frequency sweep causes only small differences in the resonance spectrum compared to an ideal profile, and hence suitable for astronomical applications.

**Keywords** Microwave kinetic inductance detectors · Readout · Telescope · Radio continuum observation

## 1 Introduction

Microwave kinetic inductance detectors (MKIDs) are resonators of superconducting film coupled to a feedline [1]. They have an intrinsic capability of frequency-domain multiplexing and are suitable for large detector arrays [2]. Power deposition into the resonator film breaks Cooper pairs in the superconductor, increasing the number

---

✉ M. Nagai  
makoto.nagai@nao.ac.jp

Extended author information available on the last page of the article

of quasiparticles, and results in changes in the resonance parameters: the resonance frequency and quality factor. The shift in the former is linear to the power for a wide dynamic range.

There are certain methods available for the readout of MKIDs (e.g., [3–6]). Though a popular method is to use the amplitude or phase of the transmission coefficient  $S_{21}$  at a single frequency in the resonance, we employed a scheme that can obtain  $S_{21}$  at many frequency points for a resonance, based on the fast Fourier transform spectrometer (FFTS) [7,8], with the frequency sweeping scheme [9]. This scheme has a dynamic range higher than the standard scheme; the probe tones can trace their target resonance even when the optical loading moves the resonance frequency significantly. Moreover, the derived resonance frequencies are not affected by changes in the gain or delay in the transmission line. Though the scheme has these advantages, the resonance profile measured can be distorted by frequency sweeping. Thus, evaluating the effect of frequency sweeping on apparent resonance spectrum is indispensable.

We made measurements using the scheme with several frequency-sweep velocities and checked the dependence of the resonance frequency and the quality factor on the sweep velocity.

## 2 Measurement

We used a 109-pixel MKID array made of a single aluminum layer on a 3-inch silicon wafer that was to be used for the radio camera to be installed on the Nobeyama 45-m Radio Telescope (Nobeyama MKID Camera), fabricated at Advanced Technology Center (ATC), NAOJ. Each MKID is a quarter wavelength coplanar waveguide (CPW) superconducting resonator [10,11], connected at its short end to a twin slot antenna for the 90–110 GHz band, and weakly coupled at its open end to the throughline. The MKID array was placed in a device holder made of Nb. To create a dark environment, the holder was closed with an Al plate and covered with radiation shields after placing it on the top load of a 0.1-K dilution refrigerator. After cooling the array below 70 mK, we found 99 resonances in the 3.3–3.8 GHz band using a vector network analyzer (VNA). We chose 4 resonances for frequency sweeping measurement, which were numbered according to their resonance frequencies (see Table 1).

The transmission spectra of the 4 resonances were simultaneously measured with the MKID readout system for the Nobeyama MKID Camera [12], whose key component is the prototype frequency sweeping probe (FSP) circuit [9]. The FSP circuit generates and acquires probe tones in base band and simultaneously sends a ramp signal to the local oscillator (LO) to modulate the frequency of the LO signal mixed with the probe tones for up/down-conversion to/from the resonator frequency band. We used one probe tone for each resonance. The LO frequency without modulation is set to 3000 MHz.

Sweep velocity,  $u$ , is determined by the FFT window duration,  $\Delta t$ , and frequency sweep step,  $\Delta f$ , as  $u = \Delta f / \Delta t$ . The FSP circuit has a fixed FFT window duration of 4  $\mu$ s. To change  $u$ , we can change the sweep step  $\Delta f = W/N$ , where  $W$  is the total modulation width and  $N$  is the number of modulation steps. We used  $N = 2^5, 2^6, 2^7, 2^8, 2^9$ , and  $2^{10}$ , and  $W = 1, 2$  and 3 MHz. The smallest and the largest

sweep steps corresponding to the values of  $N$  and  $W$  are 1.0 kHz and 93.8 kHz, respectively. Corresponding sweep velocities are in the range of 0.25–2.345 GHz/s. These sweep velocities are very high compared to a typical setup with a VNA; for example, the sweep velocity of the VNA with which we measure MKID resonance spectra is  $\sim 2.5$  MHz/s.

The FSP circuit changes the sweep direction upward and downward alternately [9]. Upward direction corresponds to the positive sign of  $\Delta f$  and  $u$ , and downward direction corresponds to their negative sign. The duration to take a spectrum is given by  $N \cdot \Delta t$ , which is equivalent to 128–4096  $\mu$ s. There is a dead time between the upward and downward sweeps of duration 0.46–3.71 ms, and the corresponding spectrum sampling rate is  $2^7$ – $2^{10}$  spectra per second for each resonance. When the sweep velocity increases, we can accordingly choose a higher spectrum sampling rate. The spectrum sampling rate used here is higher than the requirement for the Nobeyama MKID Camera,  $> 20$ – $30$  sps.

### 3 Result

We obtained the spectra of the 4 resonances successfully (Fig. 1). Each spectrum is the mean of 20 successive spectra separately calculated for upward and downward sweeps. The apparent resonance profile changes with the sweep velocity. When the sweep velocity is positive, the resonances shift upward. For higher sweep velocities, the resonance shifts increase, the apparent depths decrease, and the apparent widths increase. Similar behavior is exhibited for the negative sweep velocities. The change of apparent profile is independent of the sweep width and can be interpreted as a function of the sweep velocity or the sweep step.

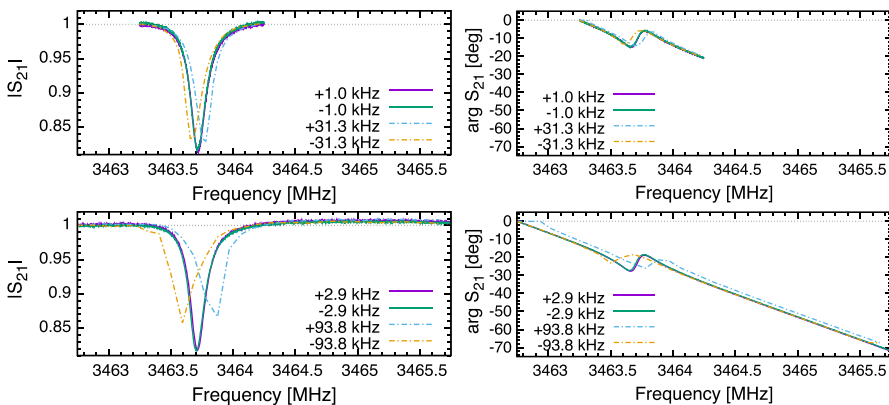


**Fig. 1** Example of spectra obtained with frequency sweeping scheme of a resonance (MKID #2). *Left* panels depict amplitude of  $S_{21}$  and *right* panels depict phase of  $S_{21}$ . *Top* and *bottom* panels are the spectra with modulation width of 1 MHz and 3 MHz, respectively. Spectra with the slowest and fastest sweep are shown. The legend indicates the frequency sweep step. The  $S_{21}$  values are normalized by its value at the probe tone origin: 3463.25 MHz for 1-MHz width and 3462.75 MHz for 3-MHz width (Color figure online)

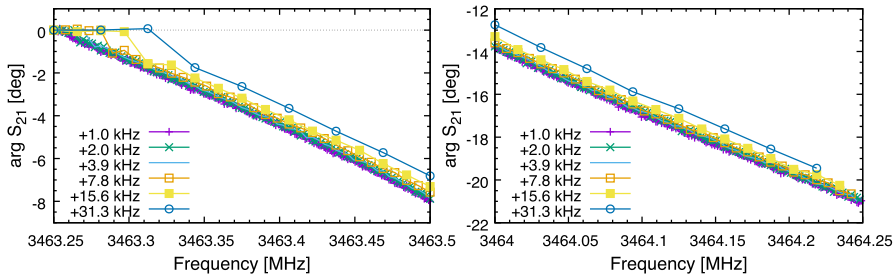


**Fig. 2** Example of phase near the ends of frequency sweeping range. Spectra of MKID #2 obtained with the upward sweep are plotted. *Left* lower end of the range, where upward sweepings start. *Right* higher end of the range, where upward sweepings end (Color figure online)

We found a distinctive feature of phase in every spectrum at the starting part of sweeping (Fig. 2). While the phase at the off-resonance points changes as a linear function of the frequency due to the cable delay and frequency conversion, there is a section where the phase stays almost constant. This feature appears at the start of sweeps: lower-frequency end of upward sweeps and higher-frequency end of downward sweeps. In contrast, the feature does not appear at the end of sweeps.

When the probe tone is swept, the LO frequency changes within a FFT window only by a factor of  $3 \times 10^{-7}$ – $3 \times 10^{-5}$ , and the sweeping, actually discrete, can be approximated by a smooth continuous motion. Then, the system is considered to be a circuit switching between a steady state of frequency-fixed tone and a frequency-sweeping tone. The phase feature at the sweep start probably occurs owing to the transition between the two states. Further analysis of transient phenomena may reveal the origin of this feature.

### 4 Discussion

To evaluate the change of the apparent resonance shape, we fitted the spectra with a skewed Lorentzian function with second-order polynomial baseline as described below. We used an amplitude fit for simplicity though there are some other fitting methods. The lower end of the frequency range,  $f_0$ , is used as an origin for baseline. For resonance, normalized frequency position for a resonator with resonance frequency  $f_r$  and quality factor  $Q$  can be defined as  $x(f; f_r, Q) = Q \frac{f-f_r}{f_r}$ . Using these defined variables, the model is given as

$$S(f; f_r, Q, a_1, a_2, c_0, c_1, c_2) = c_0 + c_1(f - f_0) + c_2(f - f_0)^2 - \frac{a_1}{1 + 2x^2} + \frac{a_2x}{1 + 2x^2}. \tag{1}$$

The fitting range is fixed in absolute values for each resonance within the range of the modulation of 1-MHz width, so that it does not affect the resulting fit. Since our interest lies in the resonance parameters  $f_r$  and  $Q$ , we did not apply scaling for amplitude values for the fit.

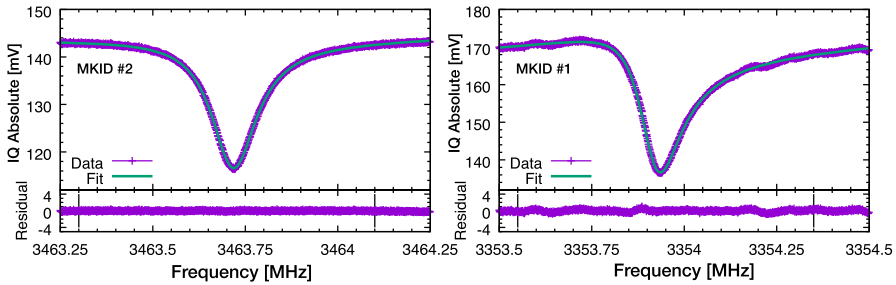


**Fig. 3** Examples of the amplitude fit. These spectra are taken with modulation width of 1 MHz and frequency step of +1 kHz. *Left* symmetric resonance. *Right* asymmetric resonance. *Black solid lines* in the *bottom* panels indicate the fitting range (Color figure online)

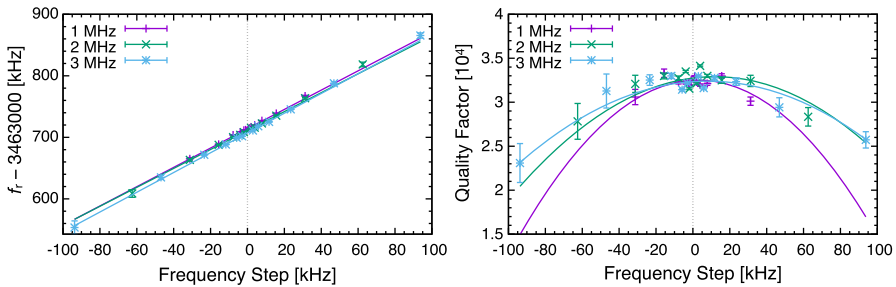


**Fig. 4** Apparent resonance parameters of a symmetric resonance (MKID #2). *Left* resonance frequency. *Right* resonance quality factor. The legend indicates the modulation width. Fitted polynomial curves (linear for resonance frequency and quadratic for quality factor) are also shown (Color figure online)

Figure 3 shows two examples of the fitting: a symmetric resonance and an asymmetric resonance. The residuals of these spectra are small. Although some spectra with larger sweep velocities have some systematic residual, the model function traces the apparent resonance shapes.

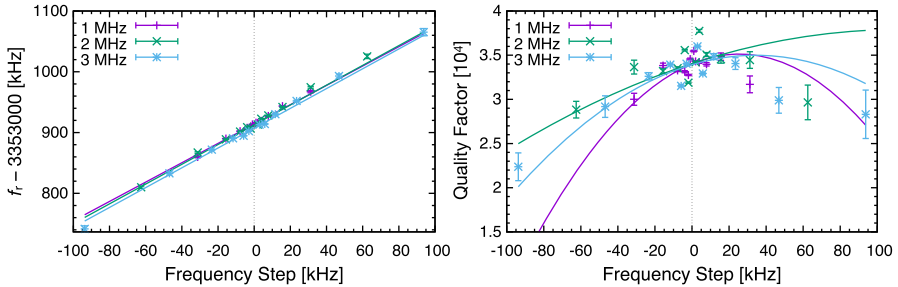
Figure 4 shows the obtained resonance parameters as a function of the sweep step. Apparent resonance frequency varies linearly with the sweep velocity for all data. Linear regression, fitting with model  $f_r(\Delta f) = f_r(0) + a\Delta f$ , was carried out, and the coefficients,  $a$ , obtained are summarized in Table 1. The values of  $a$  are almost the same, and the shift of the apparent resonance frequency can be regarded as a function of the sweep velocity.

Quality factor shows a tendency to decrease with higher sweep velocities, but with certain dispersion (right panel of Fig. 4). This dispersion partly comes from the difference in the frequency bin width. While symmetric resonances (#2, #3, #4) have symmetric shift of  $Q$  with the sweep velocity, the asymmetric resonance (#1) has asymmetric shift as shown in the right panel of Fig. 5. This result indicates that the change in the apparent quality factor is associated with the degree of asymmetry of resonance shape.

The shift in the resonance frequency can be produced by a timing difference or a delay between the probe tones generated and read. The value of coefficient,  $a$ , obtained corresponds to a timing difference of 6  $\mu\text{s}$ . The actual delay, however, is  $\sim 40$  ns for

**Table 1** Resonance parameters and coefficient of frequency shift by sweeping

MKID	$f_r$ (MHz)	$Q$	$a$		
			Modulation width 1 MHz	2 MHz	3 MHz
#1	3353.914	$3.4 \times 10^4$	$1.59 \pm 0.07$	$1.63 \pm 0.15$	$1.63 \pm 0.09$
#2	3463.714	$3.2 \times 10^4$	$1.57 \pm 0.05$	$1.54 \pm 0.06$	$1.60 \pm 0.04$
#3	3708.497	$3.8 \times 10^4$	$1.66 \pm 0.04$	$1.64 \pm 0.02$	$1.71 \pm 0.04$
#4	3733.440	$4.0 \times 10^4$	$1.71 \pm 0.07$	$1.68 \pm 0.04$	$1.72 \pm 0.04$

**Fig. 5** Apparent resonance parameters of an asymmetric resonance (MKID #1) (Color figure online)

the throughline in the cryostat and on the order of 100 ns for the whole throughline including the frequency conversion section. Thus, the delay is not the main source of the resonance frequency shift. In addition, the timing difference cannot alter the resonance shape.

The damping time constant of the resonators ( $Q/\pi f_r$ ) is  $\sim 3.2 \mu\text{s}$  and is comparable to the FFT window duration. Some interplay between the frequency sweeping and the resonator's ring up/down may occur. Models of resonator and frequency sweeping to describe the apparent resonance profiles are expected to be made.

## 5 Summary

We have simultaneously obtained 4 resonance spectra of a MKID array in a dark environment by using the frequency sweeping scheme. We found that the resonance spectra are distorted by frequency sweeping, and that the distortion is closely related to the sweep velocity. In particular, the apparent resonance frequency shift is proportional to the sweep velocity. In addition, we found a phase feature at the starting part of sweeping. Based on the dependence of the apparent resonance frequency on the sweep velocity, the exact resonance frequency can be restored by a pair of spectra taken with upward and downward sweeps. Thus, the frequency sweeping scheme can be used to operate a MKID Camera for astronomical observations, with sufficient dynamic range, stability, and sampling rate. In future work, we intend to make measurements under optical loads with the cryostat of the Nobeyama MKID Camera.


**Acknowledgements** This work was supported by JSPS KAKENHI Grant Number JP25247022, JP26247019, and JP17H01115, and was achieved using the grant of Joint Development Research (FY2017) supported by the Research Coordination Committee, National Astronomical Observatory of Japan (NAOJ), National Institutes of Natural Sciences (NINS). The authors would like to thank Shohei Ezaki and Akihira Miyachi for their assistance during MKID fabrication.

## References

1. P.K. Day, H.G. LeDuc, B.A. Mazin, A. Vayonakis, J. Zmuidzinis, *Nature* **425**, 817 (2003). <https://doi.org/10.1038/nature02037>
2. B.A. Mazin, *AIP Conf. Proc.* **1185**(1), 135 (2009). <https://doi.org/10.1063/1.3292300>
3. O. Bourrion, C. Vescovi, J.L. Bouly, A. Benoit, M. Calvo, L. Gallin-Martel, J.F. Macias-Perez, A. Monfardini, *J. Instrum.* **7**, 7014 (2012). <https://doi.org/10.1088/1748-0221/7/07/P07014>
4. S. McHugh, B.A. Mazin, B. Serfass, S. Meeker, K. O'Brien, R. Duan, R. Raffanti, D. Werthimer, *Rev. Sci. Instrum.* **83**(4), 044702 (2012). <https://doi.org/10.1063/1.3700812>
5. K. Hattori, S. Ariyoshi, M. Hazumi, H. Ishino, A. Kibayashi, S. Mima, C. Otani, N. Satoh, T. Tomaru, M. Yoshida, H. Watanabe, *J. Low Temp. Phys.* **167**, 671 (2012). <https://doi.org/10.1007/s10909-012-0506-x>
6. J. van Rantwijk, M. Grim, D. van Loon, S. Yates, A. Baryshev, J. Baselmans, *IEEE Trans. Microw. Theory Tech.* **64**, 1876 (2016). <https://doi.org/10.1109/TMTT.2016.2544303>
7. S.J.C. Yates, J.J.A. Baselmans, A.M. Baryshev, Y.J.Y. Lankwarden, L. Swenson, A. Monfardini, B. Klein, R. Güsten, in *American Institute of Physics Conference Series*, ed. by B. Young, B. Cabrera, A. Miller, vol. 1185 (2009), pp. 249–252. <https://doi.org/10.1063/1.3292325>
8. K. Karatsu, M. Naruse, T. Nitta, M. Sekine, S. Sekiguchi, Y. Sekimoto, T. Noguchi, Y. Uzawa, H. Matsuo, H. Kiuchi, *J. Low Temp. Phys.* **176**, 459 (2014). <https://doi.org/10.1007/s10909-014-1115-7>
9. H. Kiuchi, T. Okada, K. Karatsu, Y. Sekimoto, *IEEE Trans. Terahertz Sci. Technol.* **5**, 456 (2015). <https://doi.org/10.1109/TTHZ.2015.2413751>
10. M. Naruse, Y. Sekimoto, T. Noguchi, A. Miyachi, K. Karatsu, T. Nitta, M. Sekine, Y. Uzawa, T. Taino, H. Myoren, *IEEE Trans. Terahertz Sci. Technol.* **3**(2), 180 (2013). <https://doi.org/10.1109/TTHZ.2012.2237029>
11. T. Nitta, M. Naruse, Y. Sekimoto, K. Mitsui, N. Okada, K. Karatsu, M. Sekine, H. Matsuo, T. Noguchi, Y. Uzawa, M. Seta, N. Nakai, *IEEE Trans. Terahertz Sci. Technol.* **3**(1), 56 (2013). <https://doi.org/10.1109/TTHZ.2012.2235123>
12. M. Nagai, S. Hisamatsu, G. Zhai, T. Nitta, N. Nakai, N. Kuno, Y. Murayama, S. Hattori, P. Mandal, Y. Sekimoto, H. Kiuchi, T. Noguchi, H. Matsuo, A. Dominjon, S. Sekiguchi, M. Naruse, J. Maekawa, T. Minamidani, M. Saito, *J. Low Temp. Phys.* **193**(3), 585 (2018). <https://doi.org/10.1007/s10909-018-1961-9>

**Publisher's Note** Springer Nature remains neutral with regard to jurisdictional claims in published maps and institutional affiliations.

## Affiliations

M. Nagai<sup>1</sup>  · Y. Murayama<sup>1,2</sup> · T. Nitta<sup>2,3</sup> · H. Kiuchi<sup>1</sup> · Y. Sekimoto<sup>4</sup> · H. Matsuo<sup>1</sup> · W. Shan<sup>1</sup> · M. Naruse<sup>5</sup> · T. Noguchi<sup>6</sup>

<sup>1</sup> Advanced Technology Center (ATC), National Astronomical Observatory of Japan (NAOJ), 2-21-1 Osawa, Mitaka, Tokyo 181-8588, Japan

<sup>2</sup> Department of Physics, University of Tsukuba, 1-1-1 Tennodai, Tsukuba, Ibaraki 305-8571, Japan

- <sup>3</sup> Tomonaga Center for the History of the Universe, University of Tsukuba, Tsukuba, Ibaraki 305-8571, Japan
- <sup>4</sup> Department of Space Astronomy and Astrophysics, Institute of Space and Astronautical Science (ISAS), Japan Aerospace Exploration Agency (JAXA), 3-1-1 Yoshinodai, Chuo-ku, Sagami-hara, Kanagawa 252-5210, Japan
- <sup>5</sup> Graduate School of Science and Engineering, Saitama University, 255 Shimo-Okubo, Sakura-ku, Saitama, Saitama 338-8570, Japan
- <sup>6</sup> The University of Electro-Communications, 1-5-1 Chofugaoka, Chofu, Tokyo 182-8585, Japan